ENGR9700(A-D) 2021

Topic Coordinator: Dr Kristy Hansen

Evaluation of Drag Reducing Coatings

Supervisor: Professor David Lewis

Nicholas Tugwell

Thesis submitted to the College of Science and Engineering in partial fulfilment for the degree of Bachelor of Science (Chemical Sciences) (Honours), Master of Engineering (Materials), Flinders University – Adelaide, Australia

Acknowledgements

I would like to acknowledge the help of Kaili Stacey and Schannon Hamence who both helped introduce me to some of the procedures involved with the coatings in this project.
Thanks to Darren Fletcher, Fiona Cramer and Christopher Price from engineering services for their help with assembling the flow cell Device. A special thanks to Anthony Papageorgiou for his advice and help with ordering components for the flow cell device.
Finally, Professor David Lewis for his year-round support, involvement and advice in all aspects of the project.

Declaration

I certify that this thesis does not incorporate, without acknowledgement, any material previously submitted for a degree or diploma in any university, and that to the best of my knowledge and belief it does not contain any material previously published or written by another person, except where due reference is made in the text.

Executive summary

Methods of drag reduction garner significant interest from aa variety of industries, since the resultant benefits have great impact. Changing the surface of objects is an attractive method for many, since it has a passive involvement in the function of the object. Superhydrophobic surfaces offer a solution, and can be implemented relatively easily in a variety of applications.

In this project, a drag measuring device was constructed, so that a variety of coatings could be tested for their drag-reducing properties. This portion of the project made up a significant amount of the time involvement, ultimately restricting the amount of time in the end that could be devoted to gathering measurements about the nano-coatings.

Drag reduction was observed on the coatings that were tested however, it was determined that the drag reduction is likely due to the polymer present in the coating rather than the roughness. The amount of coatings tested was lower than desired.

Unfortunately, this project underachieved, in that there was insufficient amount of coatings measured and the range of reynolds numbers over which the drag was measured did not include the laminar or transitional flow regime.

Table of Contents

List of figures

1.0 Introduction

1.1 General background

Drag is the force experienced by an object as it moves through a fluid. It occurs in the opposite direction to the velocity of the object.

Two main mechanisms of drag are pressure drag and skin friction drag. Pressure drag occurs when there are two different pressure zones around the object. As the fluid slows down at the front of the object the pressure increases. The fluid moves around the object but cannot travel completely around the body of the object to the very rear, leaving a turbulent wake behind the object which is a low-pressure zone. Hence the pressure is not fully equalised, and the resultant pressure difference causes a net force in the direction opposite to the velocity of the object (Munson, 1999).

Skin friction drag is caused by the interactions of molecules at the interface between the object and the fluid. There is shear stress that occurs at the interface between the two layers, this results in momentum transfer, and hence force in the opposite direction to the velocity of the object. In general, pressure drag depends on the geometry of the shape, whereas skin friction depends on the surface morphology and energy (Munson, 1999).

Force due to drag is represented by the drag equation below [1]. F_D is force, C_D is the drag coefficient, ρ is fluid density, u is fluid velocity and A is the characteristic area of the body (Munson, 1999).

$$F_D = \frac{1}{2} C_D A \rho u^2 \qquad [1.1.1]$$

The drag coefficient is related to the shape of the object and the Reynolds number, a non-dimensional parameter that is the ratio of inertial forces to viscous forces, indicating the behaviour of the fluid flow. The Reynolds number Re can be calculated a number of ways for

example., the equation for pipe flow is shown below [2] where μ is the dynamic viscosity and *l* is a characteristic length of the body (Munson, 1999).

$$Re = \frac{\rho u l}{\mu} \qquad [1.1.2]$$

Two flow regimes are laminar and turbulent flow. Laminar flow occurs at low Reynolds numbers and can be described as flow that has a constant velocity profile. The other form of fluid flow is turbulent flow, where average velocity is maintained, but there is no layer-by-layer movement of the fluid, instead the motion of fluid particles are completely random. Laminar flow occurs at Reynolds numbers <2300 and turbulent flow occurs at Reynolds numbers >4000. Between 2300-4000 is called transitional flow, where the flow can be either laminar, turbulent or a hybrid of the two (Munson, 1999).

Riblet surfaces are a type of repetitive structure shaped like grooves along the exterior of the substrate. They were originally prepared as a biomimetic approach that are inspired by shark-skin. Sharkskin is highly textured, as shown in figure 1, which influences its abilities to move through the water quickly. (Dean and Bhushan, 2010) (Fu, Yuan and Bai, 2017)

Image removed due to copyright restriction.

Figure 1. SEM image of shark skin (Fu et al.)

The mechanism of skin friction drag reduction by textured surfaces such as shark-skin is said to occur via manipulating turbulent flow into vortices inside the grooves of the riblets, reducing momentum transfer in the boundary layer. That has the effect of redistributing the shear stress to the tips of the riblet but reducing the shear stress in the valleys, causing an

overall reduction in skin friction experienced. (Fu, Yuan and Bai, 2017) (Dean and Bhushan, 2010)

An application of deliberate texturization on a surface is the dimples on golf balls (figure 2). Golf balls can travel through the air fast enough to enter turbulent flow. The dimples on the golf ball mean that the slip length increases and the pressure equalizes more effectively between the front and rear of the ball, resulting in less drag force. The scale of the roughness is significantly greater than the focus of this project, and drag component affected is the pressure drag, rather than the skin friction drag however, it demonstrates that the benefits of roughened surfaces in relation to drag reduction have been acknowledged for some time and have broad application.

Image removed due to copyright restriction.

Figure 2. Dimpled golf ball (progolfnow.com)

Manufactured riblet surfaces have also been shown to exhibit drag reducing properties, similar to shark skin surfaces. The roughness features on the surface have the potential to reduce the drag experienced by an object by reducing skin friction drag. This occurs by reducing the shear stress at the surface of the object, which as mentioned is related to the skin friction drag.

Much research exists on riblet, textured and roughened surfaces for drag reduction however, the structures are primarily sized in the micron scale and above. Little research is gathered relating to structures at the nano scale.

The potential drag reducing benefits of nano-roughened surfaces are the motivation behind the project. Such surfaces can be prepared by using nanoparticles and a polymer based binder and are based on previous studies of the Lewis research group, where Polydimethylsiloxane (PDMS) surfaces were arranged with desired periodicity (Toster and Lewis, 2015). It is hypothesised that the texture of the nanoparticles will result in some drag reduction mechanism, analogous to the mechanisms that occur with riblets.

1.2 Significance

Drag plays a significant role in excessive energy expenditure in a variety of industries and commercial applications. For example, the benefits of drag reducing coatings will be observed in the shipbuilding industry, where the energy loss between the hull of the ship and the surrounding water contributes to significant economic and environmental cost (Dong et al., 2013). The effect of reducing skin friction drag in this scenario is a reduction in energy expenditure or increase in speed of travel, resulting in significant long-term economic and environmental benefits

Commercially there is significant interest in drag reduction for example, the Americas cup (figure 3) draws large investment regarding the optimisation of the boats used in the race. Such optimisation involves decreasing the drag of the boats in water, so that their speed, and hence performance increases.

Image removed due to copyright restriction.

Figure 3. Americas Cup racing boats (America's Cup 2012)

1.3 Research Aims

The 3 main goals of this project are as follows,

1) Construct a drag measuring system that facilitates a substrate that can be easily coated with the mentioned coatings.
2) Fabricate roughened polymer coatings on surfaces on a substrate with different roughness periodicities.
3) To evaluate the mentioned coatings for their drag reduction properties

1.4 Experimental methodology

The experimental methodology for-+this project includes fabricating polymer surfaces with varying nano-scale roughness. The surfaces will need to be tested for their drag reduction properties. The drag testing will involve constructing a flow cell that houses a coated substrate, attached to a force meter. The coatings will be deposited onto the substrate using a dip coating method and the resultant drag will be measured by the force meter.

2.0 Literature review

2.1 Outline

The focus of this review is on manufactured riblet surfaces, their effect on drag, and their real-world application. Furthermore, the methods that are used to analyse these surfaces for their drag-reducing properties. A look into current drag reducing surfaces and their durability, and ease of implementation is also included.

The gap in this literature that we will be investigating is the evaluation of nano-roughened surfaces for drag reduction. There were few resources identified that measured the effect of nano-textured coatings on drag reduction. The results of this study can contribute to the area of drag-reducing coatings and identify the benefits and drawbacks of using them. This could lead to further research into drag property measurements, fabrication of different coatings and even the application of the coatings into real world situations to take advantage of their drag reducing effects.

2.2 Shark-skin

The realisation that sharkskin has drag reduction effects has led to significant research in the area of riblet structured surfaces for drag reduction. There are also a number of other drag reduction mechanisms present in nature, such as a dolphins vibrating skin however, shark-skin is a passive drag reduction mechanism, a preferred biomimicry route since there are technologies available to produce such surfaces. Although not discussed in detail here, the riblet structure is said too also be responsible for the anti-fouling properties of shark skin, by increasing the velocity of the fluid across the surface-fluid interface. (Soleimani and Eckels, 2021)

Image removed due to copyright restriction.

Figure 4. SEM images of different species of shark-skin adapted from (Bechert, Bruse & Hage 2000)

There is a number of different shark-skin morphologies, depending on the species of shark, opening up the possibility for a variety of different fabricated surfaces for drag reduction (Figure 4).

The advantages of textured skins of sharks-skin introduces possibilities for human use of similar surfaces to achieve the same advantages. A early landmark study was performed by Walsh and Weinstein in 1979 where drag reduction was first observed on longitudinally aligned ribbed surfaces. Furthermore, the applications of the riblets can be expanded into other fluids such as air and petroleum-based liquids (Bixler and Bhushan, 2013).

2.3 Types of riblets

Riblet variables include cross-section, dimensions, and configurations. Well studied cross sections include rectangular, parabola, triangular and trapezoidal (Figure 5). (Liu et al., 1990)

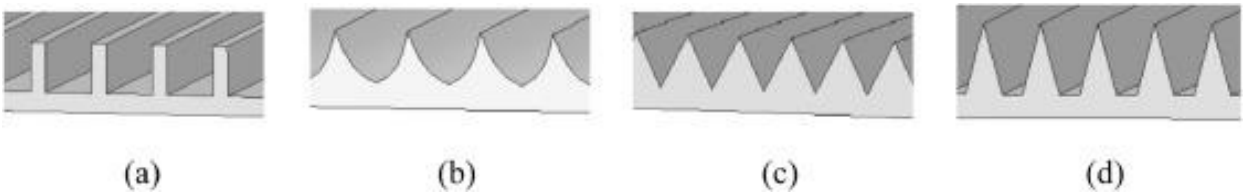

Figure 5. Riblet cross-sections; rectangular (a), parabola (b), triangular (c) and trapezoidal (d). adapted from Soleimani and Eckels, 2021

It also been shown that there is an element of riblet optimisation that may be required before employing riblet surfaces to parts. Different shapes, and dimensions are optimal for different environmental factors that include, the type of fluid, Reynolds number, surface energy factors (Soleimani and Eckels, 2021). Bechert et al performed drag reduction tests on streamwise

rectangular riblets with longitudinal ribs similar to the image in Figure 5 (a) (Bechert et al., 1997).

For further information, reviews by (Soleimani and Eckels, 2021) and (Fu, Yuan and Bai, 2017) summarise a significant portion of the literature relating to riblets and their applications.

2.4 Explanation of mechanism

The reason behind the drag reduction was observed to be as a result of the restriction of turbulent momentum transfer in the boundary layer. Restriction of the lateral momentum transfer is said to be extremely important, and this is the purpose of structures aligned in the streamwise direction.

Structures aligned perpendicular to the flow ontrol the eddies and vorticities that provide a secondary drag reduction mechanism (Figure 6). Numerical investigations also support these findings in that the riblets control the fluctuations of turbulence (Choi et al. 1993).

Image removed due to copyright restriction.

Figure 6.Turbulent vortices (Bixler and Bhushan, 2013).

2.5 Nano structured coatings literature

Combining the low wettability of superhydrophobic coatings with textured surfaces has also been examined. The combined effect can also introduce an antifouling effect, which makes them an attractive option for marine applications.

An important distinction to make at this stage is the difference between ordered and random structures. Super-hydrophobic surfaces can be fabricated with ordered or random structure (Byun et al., 2008) (Vajdi Hokmabad and Ghaemi, 2016). Random structures are coatings such as nanoparticles coatings, where there is no particular pattern observed and ordered structures can be fabricated repeatably, with some pattern. Although there is promise with ordered nano-textured surfaces, their fabrication can be difficult, and their durability is can be undesirable. (Verho et al. 2010)

Studies on the drag of random superhydrophobic surfaces indicate significant increase in slip velocity (the velocity at the interface between fluid and surface), indicating drag reduction. (Byun et al., 2008)

Drag reduction values of up to 30% in laminar and up to 15% in turbulent flows were shown to be achieved for TiO_2 nanoparticles in a hydrophobic coating. This was in comparison to a smooth aluminium disc. (Moaven, Rad and Taeibi-Rahni, 2013)

Examples of these similar coatings were prepared by Ebert and Bhushan, using dip coating to create a transparent, superhydrophobic coating with suspended nanoparticles (Ebert and Bhushan, 2012). There were no drag measurements conducted about these surfaces, a research gap that is to be addressed in this project.

Two significant authors in this field of research are Daniel Ebert and Bharat Bhushan who have contributed a significant amount to the areas of superhydrophobic coatings and drag reduction. Both are referenced multiple times in this review.

2.6 Drag Testing Methods

An example of a typical testing method is where there is some sort of closed channel, with the coating distributed on the internal surface. Two points before and after the modified surface are measured for the pressure drop, by using a manometer. Examples include Rohr, who used several sections of pipe and measured the pressure drop across 60cm of piping with

smooth and rough-coated interiors (Rohr et al., 1992). The rough-coating was a v-groove riblet coating produced by the 3 M company that was bonded inside the pipe.
Liu, used a similar method to measure pressure drop, and then calculate the friction factor of grooved triangles in 25.4mm and 50.4 mm pipes (Liu et al., 1990).

Other methods in open channel flow involve an apparatus setup with a long plate that is covered with the desired surface pattern. This is then suspended in the flowing fluid and the force due to deflection is measured. For closed channel flow, the fabricated surface can be coated in the interior of the container and the pressure drop can be measured (Figure 7).

Image removed due to copyright restriction.

Figure 7. Closed channel flow (Top), open channel flow (Bottom) adapted from Dean and Bhushan, 2010.

2.7 Conclusions

The evaluation of riblets and their drag reductions properties is important for understanding the difference between random and ordered surface structures, as well as an understanding into the mechanism behind the drag reduction.

The results of the randomly roughened surfaces that were found in the literature give a reference for the values obtained in this project.

The purpose of evaluating the drag measurement techniques in the literature is to begin to formulate a method for drag measurement in this project. Ultimately, the review revealed that a new drag measurement apparatus should be constructed for the purposes of this project (discussed further in methods).

3.0 Methods

3.1 Flow Cell Construction

3.11 Flow Cell Prototype

A prototype of the flow cell was constructed to determine if the design of the setup could effectively determine the drag on an object. The prototype also served the purpose of determining how easy it is to setup and use in practice.

25mm PVC Holman pressure pipe was purchased as well as elbows and t pieces. The device was made so that it could be attached to a tap and run on mains water. As shown in figure 8 The water flows from the tap into a horizontal section before reaching T-piece. Below the T-piece is the test section, where the specimen is held, and the piping above is to allow for any pressure head. At the top a 10N Dynanometer was held to measure the force on the specimen suspended in the flowing water.

The maximum flow rate recorded was 12L/min, resulting in a fluid velocity of 0.4m/s through the 25mm pipe. This was measured approximately by determining the time required for the water exiting the flow cell to fill up the 10 litre bucket in the sink.

A test tube was chosen as a specimen and attached to the end of the dynamometer. The prototype was not able to record any force readings however, mostly due to the insufficient resolution of the dynamometer. There were also uncertainties regarding the stability of the specimen inside the test section since it could not be observed

A follow up test was to suspend the test tube in a section of clear tube and observing its movements. This test showed that the specimen will not remain in the centre of tubing, likely

because the inner velocity is greater than the outside velocity during pipe flow, pushing the specimen to the outside of the pipe. In future experiments some way to restrict the side to side and yawing motion was required for the final design

Figure 8 Prototype – the dynamometer was held higher during experiments so that the force readings were visible

3.12 Flow cell design

The dimensions of the flow cell are dependent on a number of factors. High fluid velocities are required, and this is easier to achieve a with pipe of lower diameter however, this introduces two difficulties. Firstly, the size of the object cannot be too small because the

amount of drag force will decrease and become difficult to measure and secondly, the surface of the specimen will experience boundary effects due to its closer proximity to the wall of the pipe. The first point can be addressed by using a highly sensitive force meter however, the second point is unavoidable. As a result, there is an optimal pipe diameter that enables a large enough specimen to be used, yet also requires a less powerful pump to achieve the desired flow rates.

The maximum size of the object that can suspended in the pipe flow is determined by a commonly used rule for wind tunnels, which outlines that the object should not have a cross-sectional area of greater than 5-7% of the cross-sectional area of the pipe. (Barlow, Rae & Pope 1999)

Piping that was selected for the project was 50mm Holman PVC pressure piping and fittings. For the visible test section, 50mm polycarbonate (PC) tubing was used in place of the PVC. The joints were sealed using PVC primer and glue including the joints between the PVC and PC fittings. Figure 9 shows the final setup.

A flow meter was required to accurately measure the instantaneous flow rate during testing. Locating a flow meter that was affordable, of the correct pipe diameter and was specified to measure across a large range of flow rates was difficult. Ultimately The flow meter purchased had a 25mm diameter and was able to record the flow from 20L/min to 120L/min. The 25mm diameter was a compromise, and it had the effect of increasing backpressure throughout the system since a reducer had to be fitted to the 50mm pipe, which limited the maximum fluid velocity that could be achieved. The magnitude of this effect of this was not realised until the flow cell was constructed.

With these flow rates considered, the fluid velocity in the 50mm test section will range from 0.17 – 1.02 m/s. According to equation [2] this achieves a maximum Reynolds number of 50236.5. This is well in the turbulent regime for pipe flow

The flow meter was connected to a National Instruments (NI) counter that converted the frequency of counts to a flow rate. The data sheet for the flow meter is supplied in Appendix B.

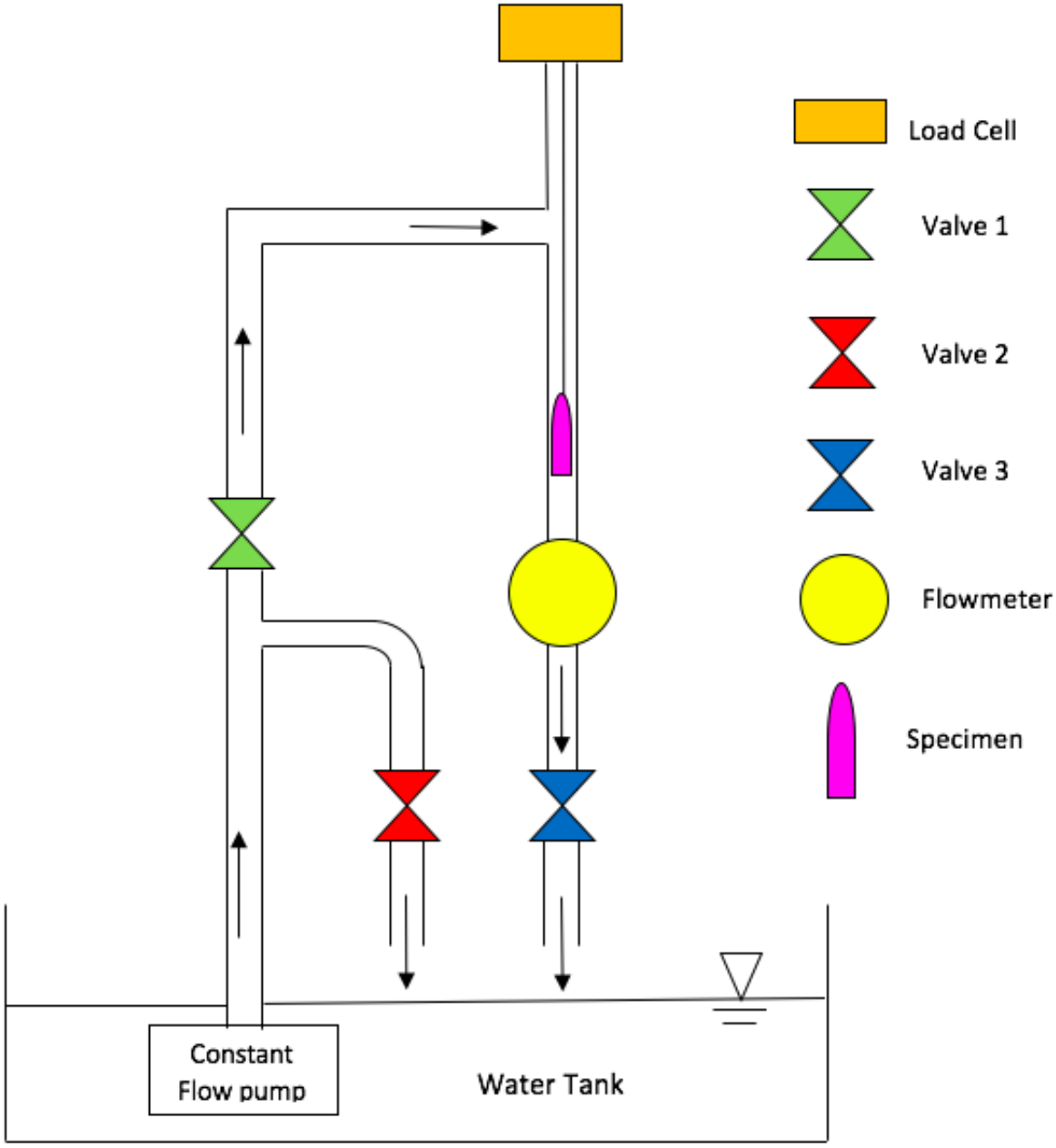

Figure 9. Schematic of the final flow cell design

The Schematic (Figure 9) depicts a simplified summary of the flow cell device outlining its workings. The beginning of the flow cell is the constant flow pump which pumps water at a constant rate towards the first T-piece. Valve 1 controls the flow of water towards the specimen, valve 2 controls the flow of water through the outlet. In practice, valve 1 was permanently left open, and valve 2 was used to reduce the flow through the outlet, subsequently increasing the flow towards the specimen. The purpose of the outlet is to reduce pressure on the pump when valve 1 is closed by allowing water to

flow back into the tank. The water flows past the specimen, through the flow meter and through valve 3. Valve 3 is also left open permanently during testing, so that the backpressure does not change and influence the flow around the specimen. The purpose of the valve 3 is to reduce the flow significantly during start-up, removing air and allowing flow to develop, before being opened completely.

The flow field around the specimen was minimally affect since is comprised less than 5% of the cross-sectional area in the test section.

*Figure 10 **T**he setup of the flow cell. (1) is the flow meter, (2) is where the load cell is positioned, (3) and (4) are the entrance and exits respectively.*

The higher of the two t-pieces on the clear PC tubing is a safety feature to prevent the water level reaching the load cell at the very top.

The load cell is position above the test section, effectively behind the flow of water to avoid as much interference around the flow of the device as possible, as will affect the record drag measurements (Figure 11).

Figure 11. Mock-up showing what the very top of the section looks like, with the PVC cap containing the load cell and the specimen suspended beneath it (left). The inside of the PVC and the load cell (right).

3.13 Entrance length of test section

With the range of testable flow rates determined by the flow meter the length of the test section can be calculated. The test section needs to allow the flow to fully develop before reaching the specimen. This is known as the entrance length and is calculated by the equation (Munson [8.2]) below

$$L_e = 4.4(D)Re^{\frac{1}{6}} \qquad [3.13.1]$$

Where D is diameter, L_e is entrance length and Re is the Reynolds number. Entering in D = 0.05m into [2] to find the Reynolds number:

$$Re = \frac{\rho v D}{\mu} = \frac{987 * 1.02 * 0.05}{1.002 * 10^{-3}} = 50236.5 \quad [3.13.2]$$

Hence the entrance length is as follows

$$Le = 0.05 * 4.4(50236.5)^{(1/6)} = \mathbf{1.34m} \quad [3.13.3]$$

The test section in the flow cell was measured to equal this length, so that when running at a maximum flow rate of 120 L/min (1.02 m/s). The specimen can be positioned far enough away from the entrance so that the flow is fully developed.

The pump purchased for this setup was a Ryobi 750W immersion pump that had a maximum flow rate of 275L/min through a 50mm outlet. Although there is some considerable height for the water to overcome, resulting in energy loss, a flow rate of double what is required was sufficient to overcome this and provide the necessary flow rates.

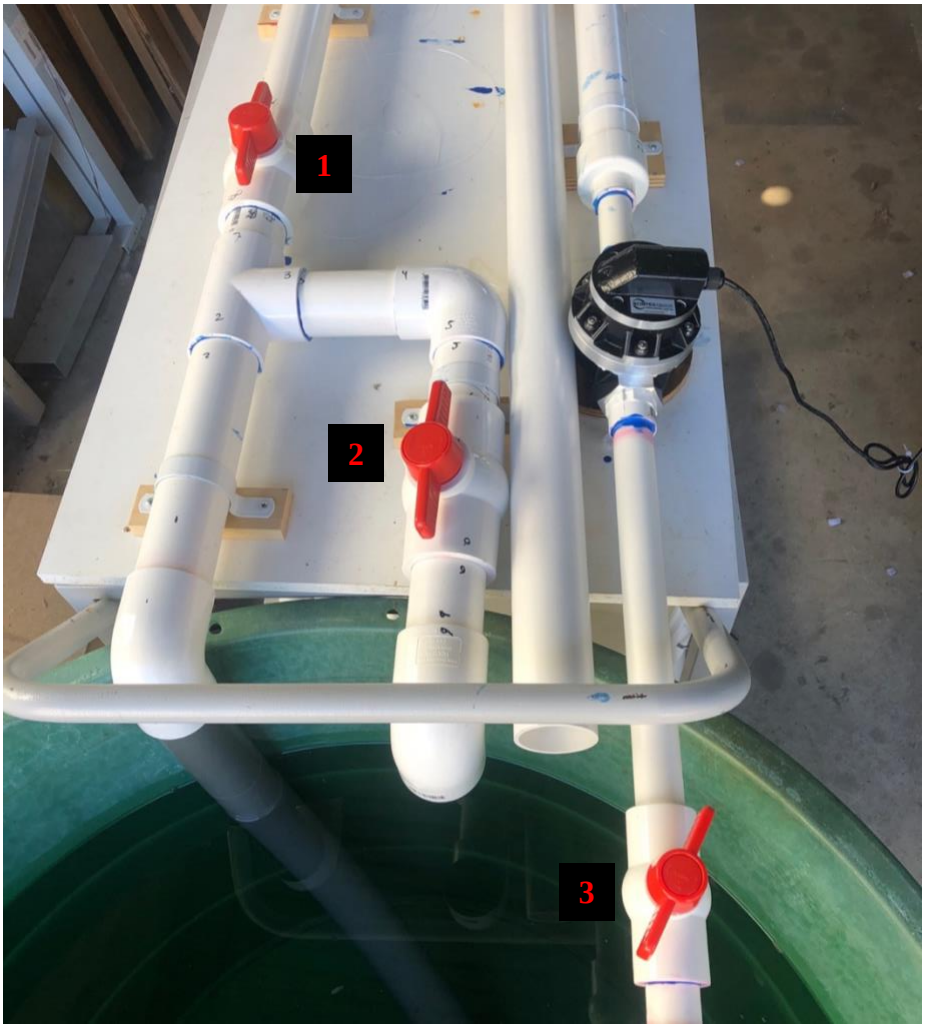

Figure 12. Valves on Flow cell

There is a series of valves that can control the flow rate through the test section. Referring to Figure 12, Valve 1 prevents any flow entering the vertical section of the flow cell, and all the water will exit out the first exit. Valve 2, located along the exit section, forces more water through the vertical section when closed, and hence through the test section. Both these valves allow for precise control over the flow rate. Valve 3 increases the backpressure throughout the system which helps the flow develop during start-up, and removes are pockets.

The pump is immersed in a large tank of water which is continuously recycled throughout the system. (Figure 13)

Figure 13. Connection of pump to flow cell

3.14 Selection of substrate

The requirements of the substrate for the coatings are

1) It must be made of a material that can be coated easily with the binder

2) The object must be in some sort of streamlined shape as to avoid a significant amount of pressure drag.

3) The object must be standardised in some way so that there is minimal difference in shape between substrates, hence less minimal variation on drag.

4) Have a cross-sectional area of less than 5% of the cross-sectional area of the 50mm pipe

Furthermore, it is ideal that the object has a streamlined shape because this will minimise the pressure drag, making the skin friction drag a larger component of the total drag, which is the component that the nanotextured coatings will affect. An airfoil shape achieves this, as it causes minimal disruption to the wake of the flow, minimizing the influence of pressure drag. Unfortunately, an airfoil shape is difficult to manufacture out of a material that can be coated effectively (such as glass).

The substrate chosen was a 10mL disposable glass test tube. Each of the test tubes had a hole drilled through the bottom to allow fishing wire to pass through with a knot tied at the other end. To prevent the excess motion of the test tube during the testing a sleeve was 3D printed that fitted to the outside of the specimen and fit snuggly within the inside of the pipe test section. (Figure 14)

With a pipe diameter of 50mm and the cross-sectional diameter of the test tube equalling 10mm, the cross-sectional areas are 490mm^2 and 19.6 mm^2 respectively, giving a ratio of 1:25 = 4%. As a result the specimen should not be significantly affected by boundary effects from the pipe wall.

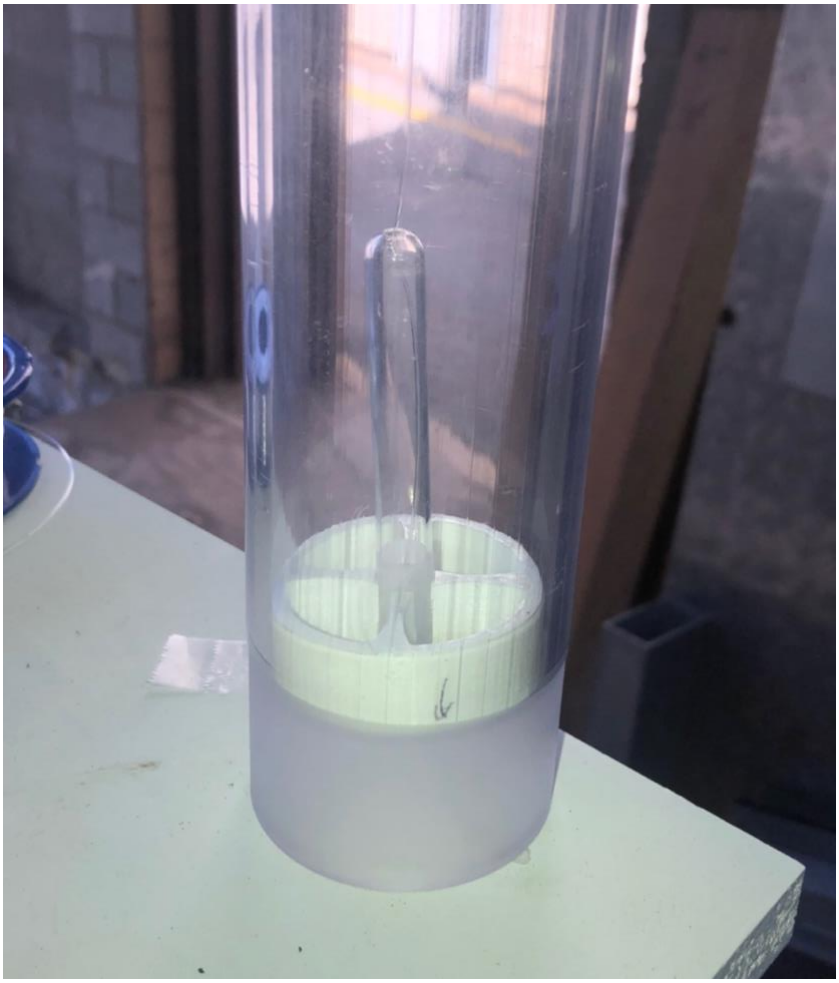

Figure 14. Demonstration of how a specimen would be held inside the test section with the attached sleeve.

3.15 Load Cell

To measure the drag on an object is to measure the force on an object. Practically, this means the specimen must be attached to a force meter of some kind. Using this particular setup, a tension load cell is ideal. So that it can be placed behind the flow direction of the object.

The drag equation was used to estimate the drag on a test tube in flowing water to give an estimation regarding the specifications of the load cell. The drag coefficient of a long cylinder was used as an approximation.

$$D_f = 0.5(\rho C_D A v^2) \quad [3.15.1]$$

A = frontal area of test tube = 3.14*10(-4)m^2

$\rho_{water\ @\ 20C}$ = 987kg/m^3

$C_{D\ sphere}$ = 0.5 (Munson)

V = 0.17m/s (minimum)

V = 1.02m/s (maximum)

$$D_f = 0.5(987 * 0.82 * 3.14 * 10^{-4} * 0.17^2) = \textbf{0.0036N}$$

$$D_f = 0.5(987 * 0.82 * 3.14 * 10^{-4} * 1.02^2) = \textbf{0.132N}$$

The drag force that is expected to be experienced by the object is within the range of 0-1N which is quite low, hence a highly sensitive load is required with a resolution of ±0.001N or greater

The load cell that was purchased was the could measure from 0-4N with a resolution of ±0.001N. The datasheet is attached in Appendix B.

3.16 Data acquisition

The load cell and flow meter was recorded simultaneously so that there was no need to manually record the flow rate every time it is adjusted. National instruments (NI) equipment along with SignalExpress software was utilised for this purpose.

The NI counter wired to the flow meter recorded the pulse output and determined the flow rate, which was displayed in real time on a laptop. Simultaneously, the load cell was connected to the NI signal express software and configured for a strain gauge type signal. The signal from the load cell was an analogue signal collect at a sampling rate of 1kHz. The force readings were also displayed in real time on the laptop. As the data was displayed, it was recorded in synchronisation, so that the force readings could be paired together with the respective flow readings for post-processing. The data was recorded in CSV format.

3.2 Procedures

3.21 Dip Coating

Solutions were prepared by adding clearcoat and nano-particles to water and mixing. Clearcoat is commercial coating based on polysiloxane chemistry. Different solutions were made through the project and these are outlined with the relevant results. Differential light scanning (DLS) was used to measure the size and distribution of the nanoparticles.

The dip coating method involved attachment of the specimen to a 3D printer arm that could move vertically at a constant rate. The coated area on the test tube needed to be standardised in some way, this was achieved by wrapping sticky tape around the opening of the test tube so that there was a marker by which the test tube was submerged to. This also served as a place where the specimens could be handled without contaminating the coatings, as well as slightly increasing the thickness of the test tube at the base so that it fit snuggly into the sleeve which is discussed below.

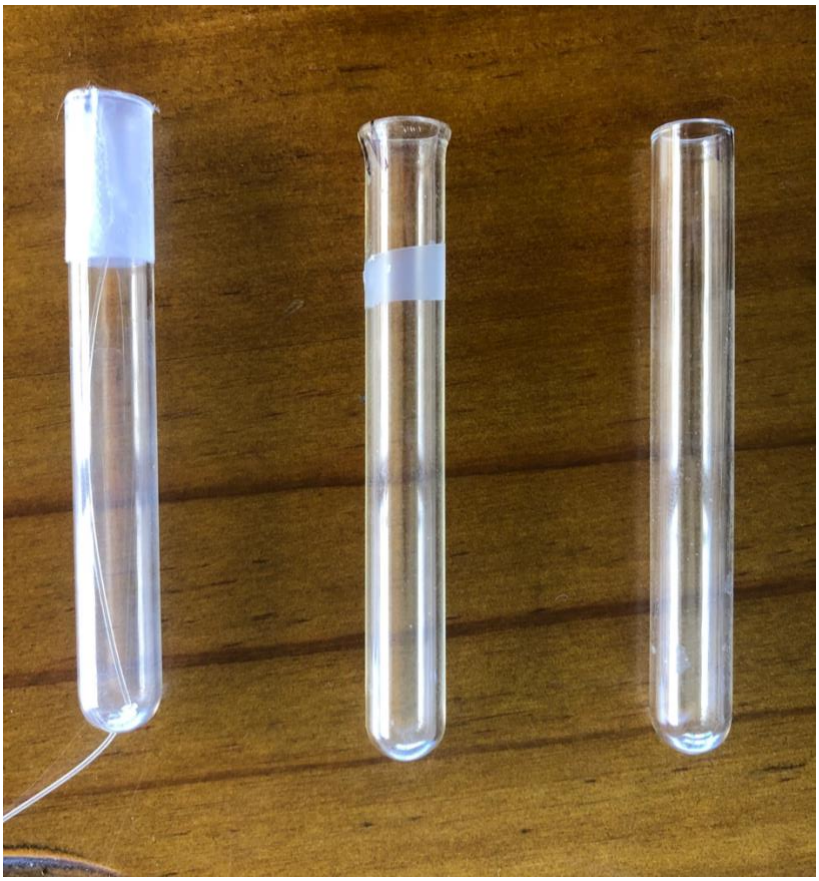

Figure 15. Test tube on the left shows how tape was attached to the end of the test tube. The middle test tube is an example a different kind with a lip at the end, and the difference can be observed by comparing it with the test tube on the right.

The test tubes were submerged for 1 minute, before being drawn out and left for 2 minutes to dry. They were placed in a 60 ^{o}C oven for 10 minutes, followed by 3hrs in an 80 ^{o}C oven. Samples were left to cool before testing in the flow cell.

3.22 Drag measurements

Before the beginning of each experience the load cell was zeroed using the SignalExpress software without any load applied. The sleeve was orientated the same way each experience to eliminate any variance that could be caused by changes in shape.

The samples were tied to the end of the load cell and suspended in the test section of the pipe. The pump is turned on the flow rate was slowly built up. The tap at the end of the system is adjusted to help remove any air that became trapped. Since there was a hole at the top of each test tube, water filled the test tube as the test continued. To ensure the weight of the test tube was consistent during the measurements, the test tube was allowed to completely fill with water before data was recorded. This typically took about 2 minutes.

Once flow had developed, the force and flow rate data were recorded. The flow rate was adjusted from the highest possible rate (approximately 64L/min) to its lowest (approximately 30L/min). The load was recorded at each of these flow rates so that the data collected could be in the form Load vs fluid velocity. Once all the flow rates had been recorded, the pump was switched of and a blank measurement of the load was recorded as the sample was suspended in the test section. This is so that the effect of the weight of the object could be accounted for, as it contributes to the total force reading on the load cell.

3.23 Experimental considerations

Temperature affects the viscosity of the water. Water at higher temperature will be less viscous and that reduce the drag on the object. Minimising the change in temperature is desired so that the force readings are not influenced. The body of water used for the experiment was quite large at almost 400L and this helped keep the temperature of the water constant. The experiment was also set up in a well sheltered garage that had relatively small temperature fluctuations. A thermometer suspended in the tank confirmed that the

temperature of the water was constant and this was checked before the beginning of every experiment to confirm.

The addition of the flow meter to the apparatus increased vibrations in the system, and the load cell was able to detect these vibrations. The effect observed was grater fluctuations in the force. The vibrations were dampened by adding extra material underneath the flow meter. The effect was most effectively minimised by taking more recordings and averaging the data. The sampling rate was set to 1000Hz hence a large number of force readings could be measured

There are some factors in the experiment that were difficult to avoid. The fishing line that was attached to the specimen will affected the drag readings as it will experience some skin friction drag. This was acceptable however, as the effects of this would be the same for every recording, and hence comparisons between specimens will not be affected by this.
The length of the fishing line was kept the same for every test, since a change in length would change its surface area, potentially influencing the results.

3.24 Data analysis

Since there was a large amount of readings a considerable amount of post processing was required. Microsoft excel was used to collate and average the data, followed by post processing, involving conversion of units. The data was then plotted and had a curve fitted, followed by integration of the curve equation.

4.0 Results

The data was in the form of flow-rate (L/min) against force (N). The flow rate was first converted to fluid velocity, and then into a Reynolds number with equation [2] using the calculated fluid velocity. The force reading was kept as is, but the weight of the specimen and sleeve was subtracted.

Reynolds number was then plotted against the drag force and a second order polynomial was fitted to the data. The resultant equation was integrated from the minimum Reynolds number to the maximum Reynolds number on the graph, the values of which were kept consistent for each sample in the same graphs. The resultant value represents the drag experienced across the flow rates, hence it is the value used to compare the total drag between samples.

4.1 Variation between test tubes

The first drag tests were to determine if the variation of drag between different test tubes was greater or similar the variation of drag due to the coatings. The substrate chosen was a test tube however, there are a number of different test tubes that are available. The drag results of using two different types of test tubes are shown in Figure 16.

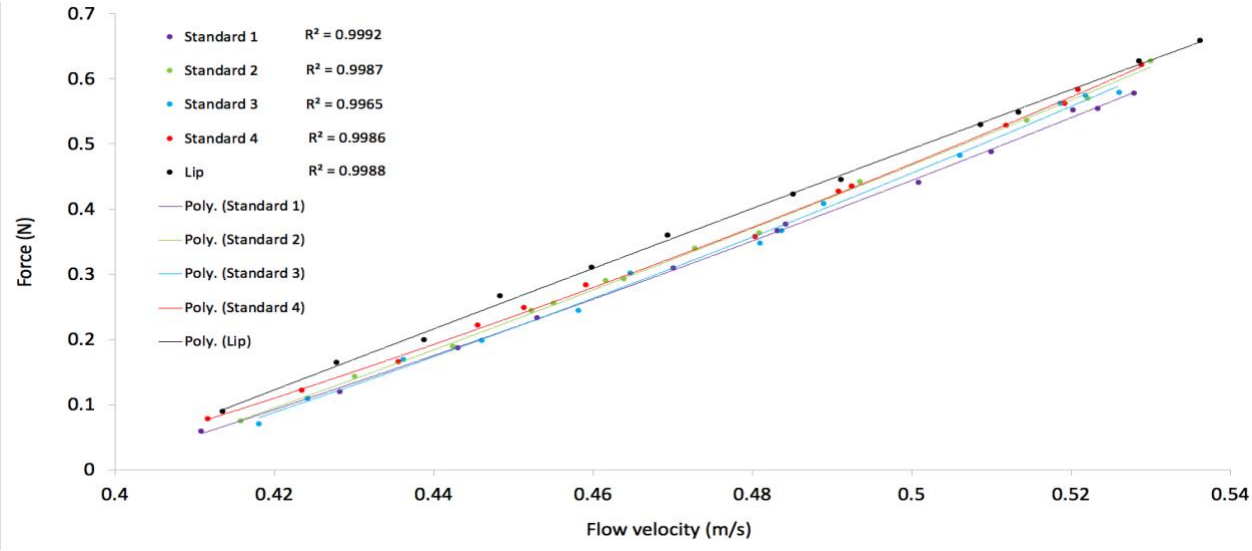

Figure 16. Drag readings of uncoated test tubes. The x axis is kept in flow velocity since it is a proof of concept test and the important information contained is the variation in force. The black is the lipped test tube

As shown in Figure 14, there can be a variation in the shapes of test tubes available. drag experienced The variation in drag between the test tubes with and without the lip was significant enough that using different test tubes interchangeably would impair the results of further tests. The small change in shape introduced by the lip is a clear demonstration of how shape also affects drag, and why consistent substrate shape is critical for valid results.

The extra lip is likely interfering with the flow around the object and it also did not fit as well into the sleeve, either of which could have influenced the results. This was a helpful test since it confirmed that the type of test tube should remain consistent throughout the experiments however, the variation between test tubes of the same type was negligible.

The data shows that repeatable data could be obtained by identical specimens. The data also was accurately described by a second order polynomial equation as all measurements had a high correlation, based on the regression values (Figure 16).

4.2 Effect of coatings

Two specimens coated with neat clearcoat were measured for their drag properties. Two other specimens were coated with a solution of 8.5% Silica nanoparticles, 4.3% clearcoat in 80% water, 20% ethanol. The drying procedure was followed as outlined in the methods. An uncoated specimen was also included in this test.

The results of the drag tests are shown below in Figure 17.

After integrating the fitted functions, it was found that in comparison to the uncoated test tubes, there was a 5.8% reduction in drag experienced by the specimen coated with the clearcoat and nanoparticles.

The difference in drag force between the clearcoat/nano-particle surface and the clearcoat only surface was 0.16%, which is negligible. The small variation observed between the textured and non-textured surfaces was not outside the variation observed between blank test tubes. Consequently, the two sets of data are not distinctive.

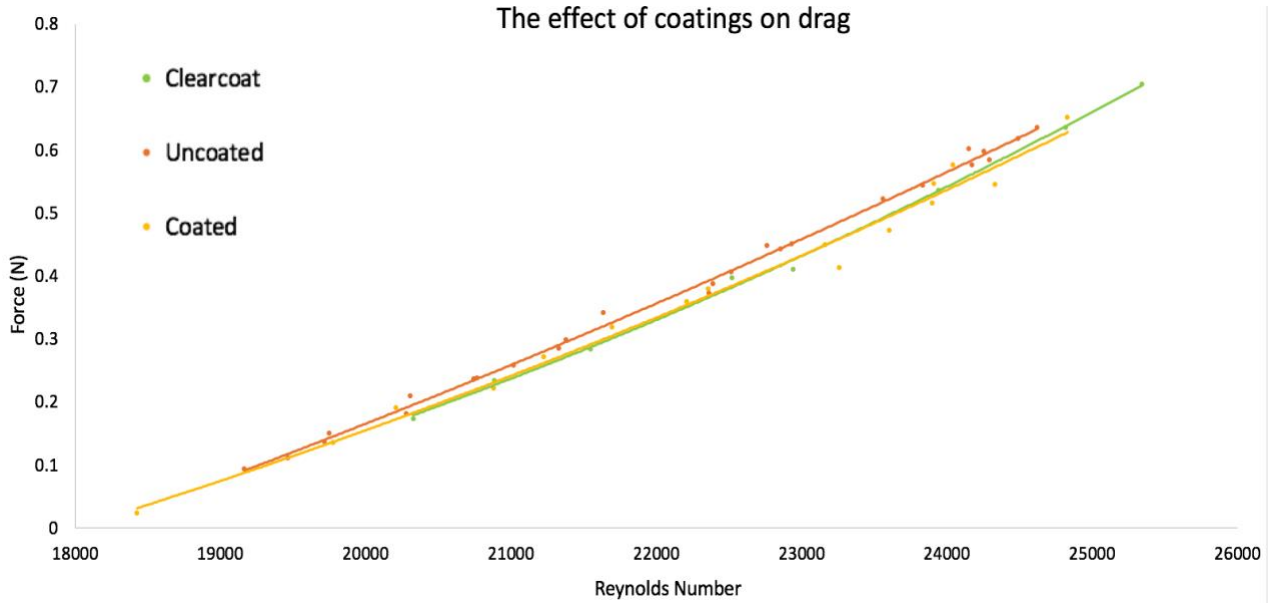

Figure 17. Force readings against Reynolds number for each coating tested

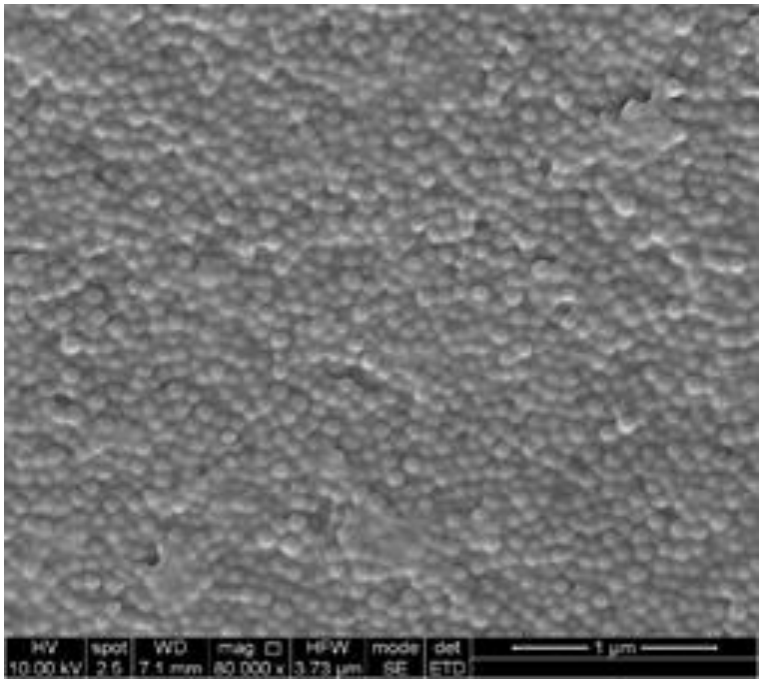

Figure 18. SEM image of the 100nm particles used to coat the specimens, thanks to Schannon Hamence for providing this image

.

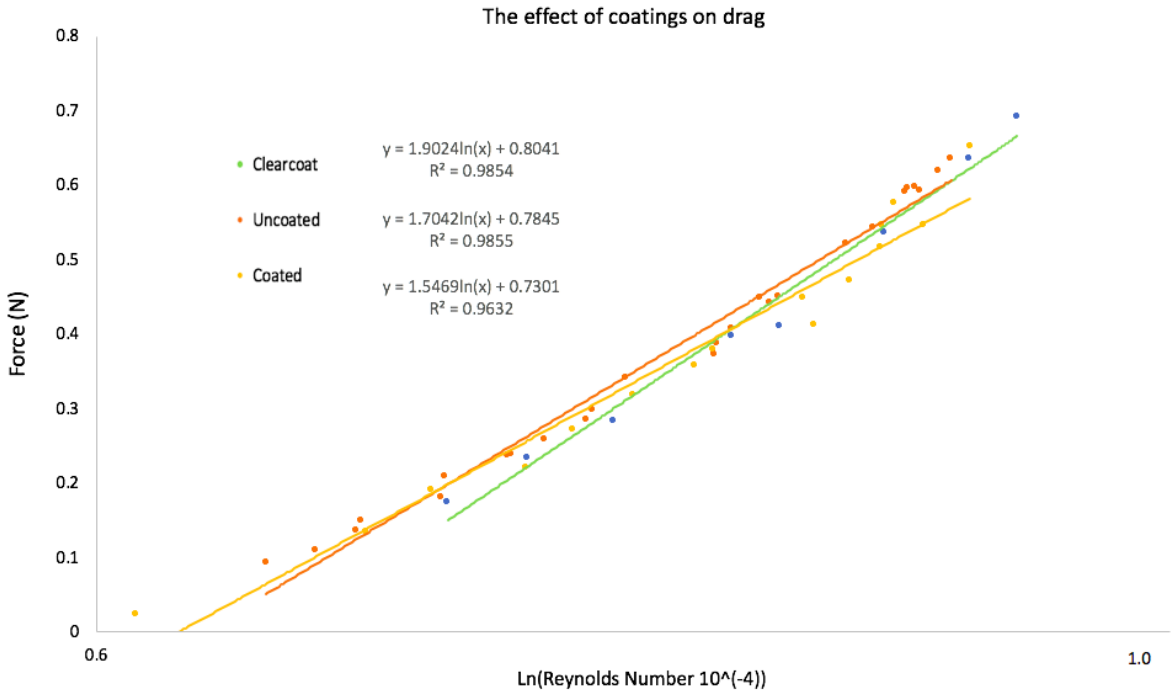

Figure 19

A log plot of Force against Reynolds number is presented in Figure 19. The fitted log curves are shown next to the respective data set in the legend. The coefficients indicate a close correlation to the second order polynomial, with the clearcoat having the closest coefficient to 2 at 1.9. This indicates that the drag measure was proportional to velocity squared, which mirrors the proportionality in the drag equation (1.1.1).

5.0 Discussion

The theoretical values calculated in the earlier stages of the project were different to the actual values recorded. 0.132N was the maximum force calculated at a Reynolds number of 50000 whereas the force recorded reached as high as 0.5N at Reynolds numbers half the value. Comparing the drag readings to calculated theoretical values is difficult for the experimental setup because the sleeve and the buoyancy of the specimen and the sleeve introduces an unknown component of force to the total force readings. This was expected and factored into the purchased of the load cell.

The data of the blank test tubes showed a strong dependency on the type of test tube that was used for each experiment due to variations in shape. The variations in drag observed in the results due to change in shape are due to changes in pressure drag.

This initial test was promising however, the variation between uncoated and coated samples needed to be well outside this range to validate. The variation between the coated and uncoated samples was significant. As shown in Figure 14 the uncoated and coated samples are clearly two different data sets. This validates the data, since it can be concluded that the changes in force readings are due to the addition of coatings rather than variations within the test tubes.

Critically, there was no significant force reduction observed between samples with and without nanoparticles, implying that the nano-scale texture had no measurable effect on the drag experienced by the samples. The possibly real-world applications are thus due to the clearcoat surface and not the nano-textured coating.

5.1 Significance

The effect of the coating was a 5.8% reduction in force. A 5.8% reduction in force required to achieve a certain velocity can result in significant energy savings in real world applications. Depending on costing, durability and other factors, this amount of drag reduction could be desirable.

The drag tests were all performed in turbulent flowing water, as the force readings were inaccurate at flow rates that corresponded to laminar flow. The buoyancy of the specimen and sleeve was responsible for this interference as mentioned. This unfortunately means that drag experienced over the transitional flow period wasn't observed during these experiments.

It was expected that as the flow increased into the transitional flow regime there would be decrease in drag force observed, the roughened surface experiences lower drag in the

turbulent regime. Furthermore, the effect of roughened surfaces is more pronounced in the turbulent region because of their reduction of momentum transfer in the turbulent boundary layer.

Other limitations include the variety of coatings that that were measured for drag reduction. Different binders (such as PDMS) could be explored to determine how different this affects the drag force. Other nanoparticle sizes could also be explored, as this affected the texturization of the surface, as well as different distributions of nanoparticles sizes. Furthermore, particle sizes closer to a micron in size could be used in place of nano-particles.

5.2 Limitations

The limitations of this research are that the span of Reynolds numbers over which the drag was measured was small. Particularly because only turbulent flow was measured, when ideally laminar and transitional flow could have been explored.

Another area that should be addressed is durability measurements to determine how well these coatings stay attached to surfaces and/or if the drag properties are changed over extensive time. the data we have recorded will be irrelevant to most applications if durability is questionable.

A significant limitation of these results is the lack of quantification of the riblet heights. The procedure is repeatable, and will consistently produce the same coatings however, there is no data on how the roughness was quantified. In typical riblet studies, this is by the riblet heights and widths with respect to the viscosity of the fluid. In this study we have not measured the roughness in this way, making the results hard to compare against other studies.

An example of a wear testing procedure that could be following was outlined by (Stenzel, Wilke & Hage 2011) in their paper regarding drag reducing paints for aviation. Firstly, the coating was applied to a test surface. The test surface (in this instance an aircraft wing) was

put into operation for 1 year. The surface was monitored at regular intervals to determine the change in surface due to wear by SEM imaging.

Addressing these limitations will give a greater indication to the potential usefulness of these coatings in real world applications.

A limitation of these experiments is that they are not compared against benchmark values. There is little area for comparing against a benchmark value since there is no standardised method of measuring drag. This is evident in the literature whereby many different methods are used to measure drag properties of objects and surfaces etc.

6.0 Conclusions

A drag measuring device was constructed that was suitable for detecting small changes in drag experienced by a specimen immersed in nano-textured coatings. The construction of this device took up the majority of the project.

Glass test tubes were coated with polymer/nanoparticle coatings and used to measure the reduction in drag that the nano-coatings are responsible for. A drag reduction of 5.8% was observed however, eliminating the nanoparticles also gave a 5.8% reduction, indicating that the roughness features were not responsible.

There are limitations to this project that should be addressed before reaching this conclusion in full including, increasing the span of Reynolds numbers over which the drag is measured and including more variety of nano-particles in the coatings tested.

7.0 Future work

Measuring the drag reduction effects over a range of Reynolds numbers should be undertaken, Particularly turbulent Reynolds numbers as there has been a great deal of drag reduction observed in the turbulent regime as mentioned in the literature review.

There are broad variety of nano-roughened surfaces that could be tested for their drag reduction possibilities. Differently sized nanoparticles could be included in the coating,

ultimately influencing the roughness on the surface of the substrate. This could affect the shear stress reduction mechanisms such as vortices and hence affect the drag.

Bi-modal distributed sized nanoparticles could be used in a coating to determine how this particular roughness scheme influences drag.

Long-term durability of these coatings in flowing water is an unknown. This should be tested because there would be little interest in pursuing such coatings if they decay over time and/or their drag reduction effects reduce.

These coatings could be tested in other media such as air or petroleum-based liquids. The drag properties of these coatings in other media is unknown, as well as their durability, as it is possible that the media influences this also.

8.0 References

Acushnet introduces Union Green golf balls and takes a giant divot 2020, Pro Golf Now.

America's Cup 2012, THE TECHNOLOGY, 36th America's Cup presented by PRADA.

Barlow, JB, Rae, WH & Pope, A 1999, Low-speed wind tunnel testing, Wiley, New York.

Bixler, G.D. and Bhushan, B. (2013). Shark skin inspired low-drag microstructured surfaces in closed channel flow. *Journal of Colloid and Interface Science*, 393, pp.384–396.

Bruce Roy Munson, Huebsch, W.W., Okiishi, T.H. and Young, D.F. (2012). *Fundamentals of fluid mechanics*. Hoboken, New Jersey: John Wiley & Sons, Inc.

Byun, D., Kim, J., Ko, H.S. and Park, H.C. (2008). Direct measurement of slip flows in superhydrophobic microchannels with transverse grooves. *Physics of Fluids*, 20(11), p.113601.

Choi, H., Moin, P. and Kim, J. (1993). Direct numerical simulation of turbulent flow over riblets. *Journal of Fluid Mechanics*, 255(-1), p.503.

Dean, B. and Bhushan, B. (2010). Shark-skin surfaces for fluid-drag reduction in turbulent flow: a review. *Philosophical Transactions of the Royal Society A: Mathematical, Physical and Engineering Sciences*, 368(1933), pp.5737–5737.

Ebert, D. and Bhushan, B. (2012). Transparent, Superhydrophobic, and Wear-Resistant Coatings on Glass and Polymer Substrates Using SiO2, ZnO, and ITO Nanoparticles. *Langmuir*, 28(31), pp.11391–11399.

Fu, Y.F., Yuan, C.Q. and Bai, X.Q. (2017). Marine drag reduction of shark skin inspired riblet surfaces. *Biosurface and Biotribology*, 3(1), pp.11–24.

Liu, K.N., Christodoulou, C., Riccius, O. and Joseph, D.D. (1990). Drag reduction in pipes lined with riblets. *AIAA Journal*, 28(10), pp.1697–1698.

Moaven, Kh., Rad, M. and Taeibi-Rahni, M. (2013). Experimental investigation of viscous drag reduction of superhydrophobic nano-coating in laminar and turbulent flows. *Experimental Thermal and Fluid Science*, 51, pp.239–243.

Rohr, J.J., Andersen, G.W., Reidy, L.W. and Hendricks, E.W. (1992). A comparison of the drag-reducing benefits of riblets in internal and external flows. *Experiments in Fluids*, 13(6), pp.361–368.

Soleimani, S. and Eckels, S. (2021). A review of drag reduction and heat transfer enhancement by riblet surfaces in closed and open channel flow. *International Journal of Thermofluids*, 9, p.100053.

Stenzel, V., Wilke, Y. and Hage, W. (2011). Drag-reducing paints for the reduction of fuel consumption in aviation and shipping. *Progress in Organic Coatings*, 70(4), pp.224–229.

Vajdi Hokmabad, B. and Ghaemi, S. (2016). Turbulent flow over wetted and non-wetted superhydrophobic counterparts with random structure. *Physics of Fluids*, 28(1), p.015112.

Verho, T., Bower, C., Andrew, P., Franssila, S., Ikkala, O. and Ras, R.H.A. (2010). Mechanically Durable Superhydrophobic Surfaces. *Advanced Materials*, 23(5), pp.673–678.

Walsh, M.J. and Weinstein, L.M. (1979). Drag and Heat-Transfer Characteristics of Small Longitudinally Ribbed Surfaces. *AIAA Journal*, 17(7), pp.770–771.

Appendix A (Images)

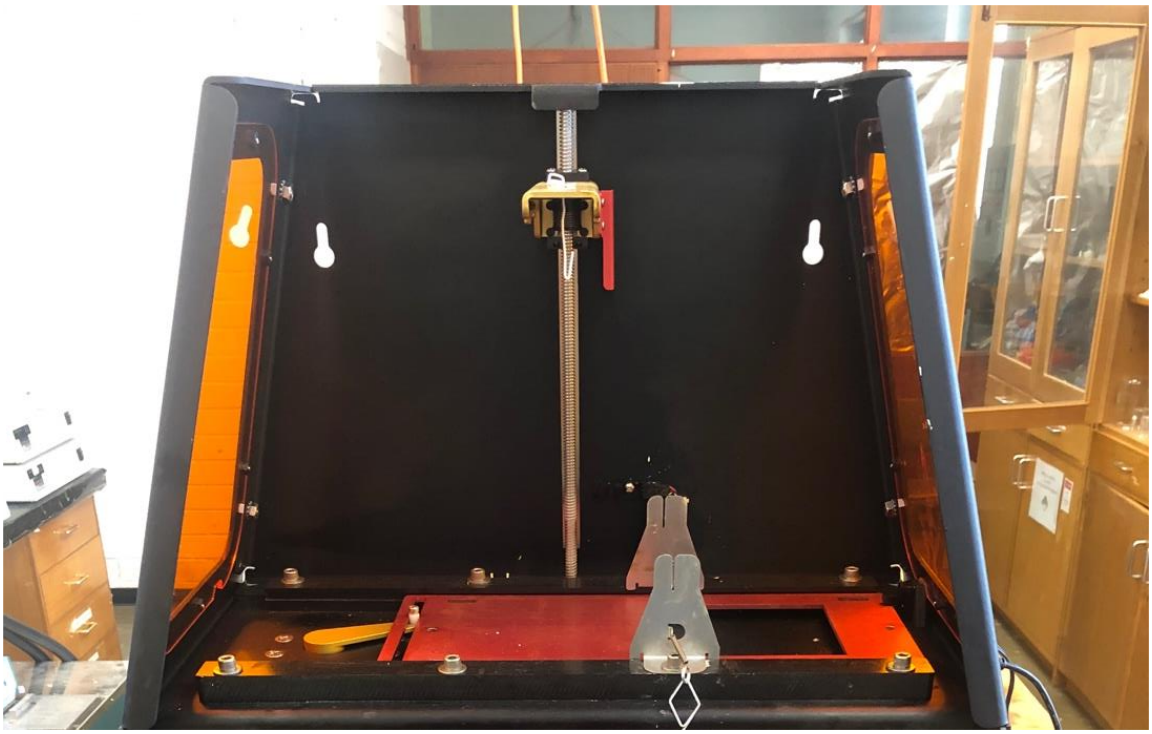

Figure 20. the specimens were suspended from the yellow arm in the centre. The arm moves down the screw at a constant rate

Figure 21. 10 N dynamometer used for protoype experiments

Figure 22. Front on view of the flow cell

Figure 23. Side view of flow cell

Figure 24. National instruments counter that was connected to the flow cell

Figure 25. Flow meter

.

Appendix B - Datasheets

Flow meter Datasheet

Flow Meter Specification	SPEVOGMA25 / SPEVOGMB25 / SPEVOGME25
Inlet / Outlet	1" BSP
Minimum Flow Rate	20 L/min
Maximum Flow Rate	200 L/min
Accuracy	+/- 0.5%
Repeatability	<0.03%
Maximum Viscosity Rating	1000 CPS
Maximum Operating Pressure	1.8 MPa, 261 psi (SPEVOGMB25 /3.4 MPa, 490 psi)
Construction	Aluminium
Functions	Totaliser, Total Reset
Options	Optional pulse output model (SPEVOGMB25) 5-36v DC 15 mA draw 0.048 L/rev Optional digital display model (SPEVOGME25)
Dimensions	140mm (W) x 170mm (D) x 110mm (H)
Warranty	12 Months

ME-Meßsysteme GmbH
Eduard-Maurer-Str. 9
DE-16761 Hennigsdorf

Tel +49 (0)3302 8982 4 10
Fax +49 (0)3302 8982 4 69

Mail info@me-systeme.de
Web www.me-systeme.de

Dimensions

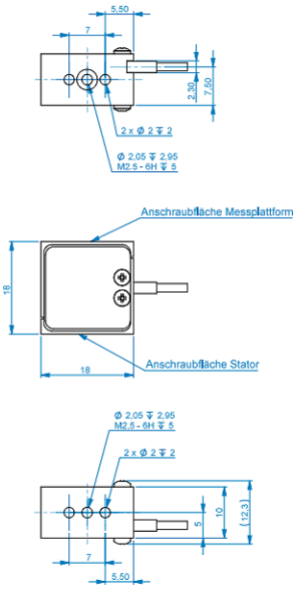

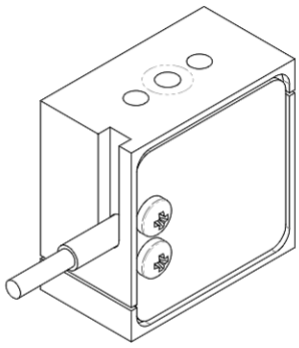

Variante mit Kabel horizontal

ME-Meßsysteme GmbH
Eduard-Maurer-Str. 9
DE-16761 Hennigsdorf

Tel +49 (0)3302 8982 4 10
Fax +49 (0)3302 8982 4 69

Mail info@me-systeme.de
Web www.me-systeme.de

Technical Data

Force sensor		
Type	Force sensor	
Force direction	Tension / Compression	
Rated force Fx	2	N
Force introduction	Inner thread	
Dimension 1	M2,5	
Sensor Fastening	Inner thread	
Dimension 2	M2,5	
Operating force	200	%FS
Rated displacement	0.2	mm
Lateral force limit	100	%FS
Material	Aluminium alloy	
Natural frequency	1	kHz
Height	18	mm
Length or Diameter	18	mm

Electrical Data		
Input resistance	390	Ohm
Tolerance input resistance	40	Ohm
Output resistance	350	Ohm
Tolerance output resistance	1.5	Ohm
Insulation resistance	5	GOhm
Rated range of excitation voltage f	2.5 ... 5	V
Operating range of excitation voltage f	1 ... 10	V
Zero signal	0.05	mV/V
Rated output	0.5	mV/V / FS

Precision		
Relative linearity error	0.02	%FS
Relative zero signal hysteresis	0.02	%FS
Temperature effect on zero signal	0.02	%FS/K
Temperature effect on characteristic value	0.01	%RD/K
Relative creep	0.1	%FS

Connection Data		
Connection type	4 conductor open	
Name of the connection	STC-32T-4	
Cable length	3	m

Temperature		
Rated temperature range f	-10 ... 70	°C
Operating temperature range f	-10 ... 85	°C
Storage temperature range f	-10 ... 85	°C
Environmental protection	IP65	